D027

Fracture Network Growth for Prediction of Fracture Characteristics and Connectivity in Tight Reservoir Rocks

A. Barnhoorn* (Delft University of Technology) & S.F. Cox (Australian National University)

SUMMARY

Fracturing experiments on very low-porosity dolomite rocks shows a difference in growth of fracture networks by stress-driven fracturing and fluid-driven fracturing. Stress-driven fracture growth, in the absence of fluid pressure, initially forms fractures randomly throughout the rocks followed by growth and coalescence of fractures to form a connected fracture network. Fluid-driven fracture growth is represented by preferential fracture growth occurring initially at the high fluid pressure part of the rock. With prolonged durations of high fluid pressure at the tip of the newly formed fractures, the network propagates rapidly through the sample and away from the high fl uid pressure reservoir. This difference in fracture network growth and the differences in fracture statistics between both scenarios have important control on the flow of hydrocarbons in fractured reservoirs and thus on hydrocarbon productivity. Differences in fracture statistics can eventually be used as improved input into reservoir and production models. 3D X-ray tomography analyes of a fractured specimen show very early 3D fracture connectivity, much earlier than depicted from conventional 2D analyses. The early 3D connectivity of fractures and enhanced permeability may also be critical to the understanding of hydrocarbon storage and migration or seal integrity.

Introduction

Faults and fractures play a major role in a wide variety of tectonic processes on Earth such as earthquake nucleation, channelling of magmas during volcanic eruptions and act as planes along which movement is focussed in orogenic processes. Fault and fractures also have important economic consequences such as in ore mineralisation along faults in hydrothermal systems (e.g. gold), accumulation of hydrocarbons in reservoirs, integrity of reservoirs (Aydin, 2000).

Interaction between fractures and fluids flowing through networks of fractures causes changes in fault permeability due to formation of reaction products on fault surfaces, dissolution of fault material into fluids, or propagation of fracture networks. Fluid pressure gradients in tectonically stressed faults may even enhance failure. Movement of such high pressure fluids along fractures has been interpreted to drive earthquake and aftershock activity (Miller et al., 2004, Sibson, 2007). Propagation of high fluid pressures along fracture networks is also employed by industry to enhance productivity in poorly producing conventional petroleum reservoirs (EOR: Enhanced Oil Recovery, e.g. Babadagli, 2003), in the newly developing unconventional shale oil/gas exploration where hydraulic fracturing induces flow in initially very low permeable shales (e.g. Curtis, 2002) and in geothermal reservoir stimulation (Baisch et al., 2006).

In particular, at the percolation threshold, when the growth of fractures creates first a connected network of fractures, drastic changes in both mechanical and fluid transport properties and thus productivity of hydrocarbons from reservoir rocks can occur. It has been suggested that fracture networks may evolve differently (Figure 1) when high fluid pressures and fluid pressure gradients are present with respect to the case where no fluids, or fluid pressure gradients are present. Cox (2005) postulated that fracture growth in isotropic rocks driven by stress changes (no fluid pressure gradients) is characterised by fracture generation randomly throughout the sample when stresses exceed the yield strength of the rock. During continuing fracturing, more fractures nucleate and fractures grow eventually forming a connected fracture network. In the presence of high fluid-pressure gradients and at differential stresses smaller than the dry yield strength (i.e., no fractures yet present), an increase in fluid pressure can reduce the effective pressure leading to failure (hydraulic fracturing). Maintaining elevated fluid pressures at the tip of the fractures, may results in continuation of failure and propagation of the fracture network into the rock mass. The difference between these 'stress-driven' and 'fluid-driven' fracture generation scenarios may have important differences resulting in differences in the distribution of fractures in fractured hydrocarbon reservoirs. Both the difference in fracture distribution in two-dimensional sections through rock masses as well as the real three-dimensional distribution of fractures may be distinctly different for both scenarios. Understanding of the differences in fracture distribution and statistics for both scenarios may help improving prediction of flow of hydrocarbons along natural fracture networks or generated fractures due to hydraulic stimulation procedures.

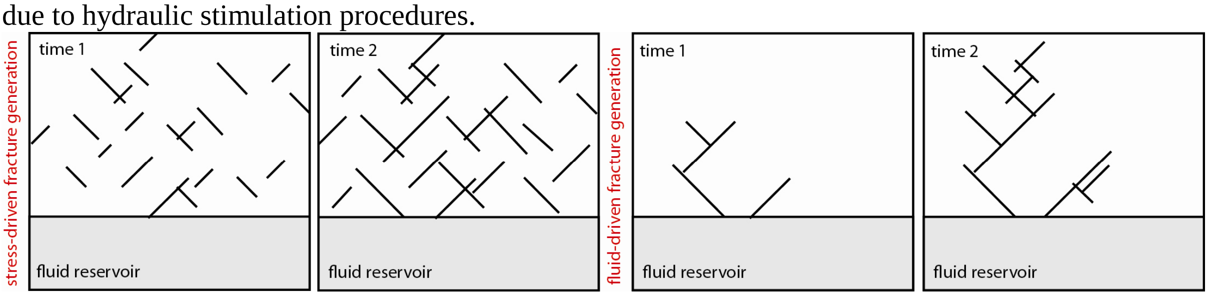

Figure 1 *Schematic diagrams showing the differences between stress-driven and fluid-driven fracture generation (adapted from Cox, 2005).*

In this study, those two types of fracture network growth processes have been produced experimentally in the laboratory under controlled conditions of pressure, temperature, differential stress and fluid pressures. Experiments have been terminated at different stages in the fracture forming process both in the presence and absence of high fluid pressure gradients. The fracture distribution along two-dimensional sections through the sample as well as a 3D visualisation of fractures using micro X-ray tomography have shown difference in the formation of fracture networks and fracture statistics for both fracture formation scenarios.

Method

Deformation experiments were conducted on low-porosity dolomite specimens with a length *l* ~22 of mm and a diameter of 10 mm. Before fracturing, the specimens contained no visible porosity on optical thin-sections and in the Scanning Electron Microscope. Thus before fracturing, permeability can be considered to be very low as well. Specimens were deformed in a Paterson gas apparatus in which confining pressure, fluid pressure and compressional defomation rate (strain rate) can be independently controlled. Two types of triaxial deformation experiments were performed at room temperature: 1) Brittle failure driven by increasing differential stress at nominally constant strain rate in the absence of a pore fluid, 2) Brittle failure driven by increasing fluid pressure at one end of the sample at approximately constant differential stress.

First, the confining pressure was raised to 50 MPa (experiments without a pore fluid) or 100 MPa (experiments with a pore fluid). Specimens were then shortened axially at a nominal strain rate between $2x10^{-6}$ s^{-1} to $1x10^{-5}$ s^{-1}. In the absence of fluid pressures, stresses were increased beyond the yield strength of dolomite and then halted at different strains ranging from the onset of generation of the first fractures to failure of the sample and generation of a throughgoing shear fracture. In the fluid experiments with high fluid pressure gradients, loading of the specimens was stopped at stresses just below the yield strength of dolomite. Subsequently fluid pressures at the top of the specimen were raised to typically 0.5–0.8 of the confining pressures and those high fluid pressures were maintained for periods up to several minutes. Continuous high fluid pressures and continuous supply of fluids caused propagation of the fractures away from the top of the sample (fluid reservoir). Drained conditions at the bottom allowed fluids to escape and prevented the build-up of significant fluid pressure at the bottom of the sample, thereby maintaining high fluid pressure gradients across the specimen.

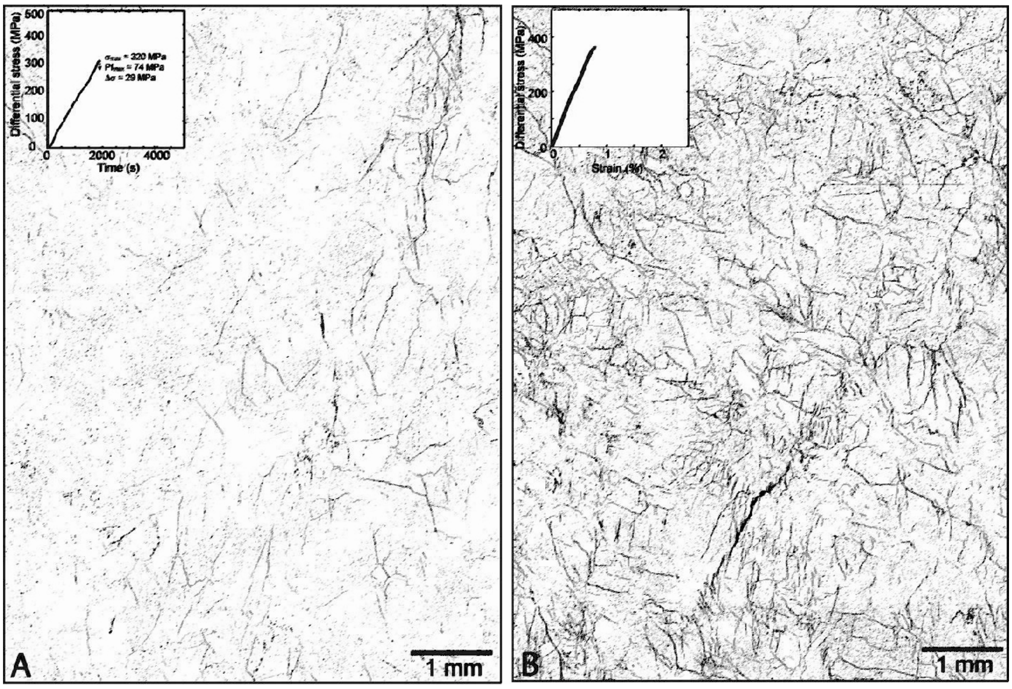

***Figure 2** Fracture networks in experimentally deformed low-porosity dolomite. A) Fracture network growth due to the presence of an elevated fluid H_2O pressure at the top of the specimen. B) Fracture network growth in the absence of elevated fluid pressures. Random fracture generation due to the applied differential stresses.*

Grayscale images of the samples obtained using backscattered electron imaging (BSE) in a scanning electron microscope were thresholded to produce images in which fractures are represented by black pixels and white pixels represented unfractured dolomite (Figure 2). Analyses using MATLAB object recognition and connectivity routines provided statistical estimates of fracture densities (the fraction of the area taken up by black pixels; i.e., fractures) across the sample, fracture lengths, orientation, and fracture abundances (number of fractures present). One specimen deformed to peak stress conditions in the absence of elevated fluid pressures was analysed using

3-D microcomputed X-ray tomography (Sakellariou et al., 2004). A cylinder with a diameter of 2.5 mm and a length of 5 mm was cored from the specimen and imaged using X-rays over a 360° rotation with 0.125° intervals. Density contrasts between dolomite and fractures (voids) were depicted by the analysis and a 3-D image of the fracture network was constructed. Connectivity analysis determined whether individual fractures belong to a connected 3-D fracture network.

Examples

Figure 2 shows the difference in fracture formation in the absence and presence of elevated fluid pressures. In the presence of high fluid pressure gradients (Figure 2A) fractures form at the high fluid pressure end of the specimen (top) and propagate downwards away from the fluid reservoir. The fracture density is also highest at the top end of the specimen (Barnhoorn et al., 2010) and decreases downwards. Dominant fracture orientation of the specimen formed by fluid-driven fracturing show predominantly near vertical to 70° fractures (Figure 3). Fracture networks formed by stress-driven fracturing (Figure 2B) are characterised by the random generation of fractures throughout the sample. No significant differences in fracture density occurs from the top to the bottom of the specimen. Those randomly generated fractures grow and link forming eventually a throughgoing fracture network. The specimen illustrated in Figure 2B has been loaded till peak stress conditions at which in two-dimensions full fracture connectivity has not yet been attained. The dominant fracture orientations show in addition to ~70° shear fracture orientation, a conjugate set of fractures at ~30° occurs that is absent in the fluid-driven scenario.

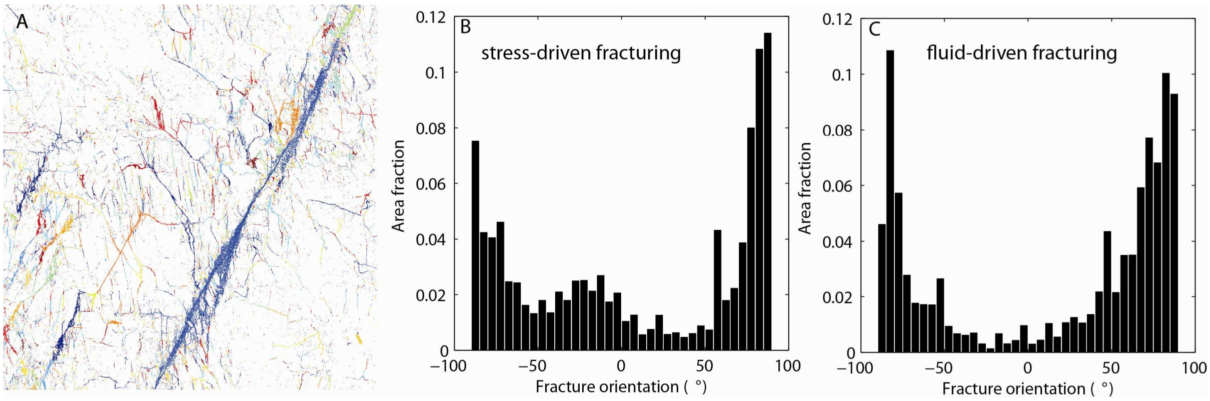

Figure 3 *Fracture statistics for stress-driven and fluid-driven fracturing: A) All individual fractures (not-connected in 2D) have been assigned an specific colour B) and C) Histograms of fracture orientation for stress-driven and fluid-driven fracturing experiments. An orientation of 0° is horizontal .*

Three-dimensional analyses using micro X-ray tomography (Figure 4) shows that the fracture network formed by stress-driven fracture growth contains one network of connected fractures in three dimensions, whereas in two-dimensions a connected network was not yet visible (Figure 2B). This early, 3D connectivity shows that fluids/hydrocarbons can migrate along fractures much earlier than previously thought. Shear failure of the samples is not needed for increased fluid flow along tortuous 3D pathways and increased permeabilities are thus expected at very low fracture densities.

Conclusions

The differences in fracture network growth and fracture statistics in the absence and presence of fluid pressure gradients may have important control on the flow of hydrocarbons in fractured reservoir and thus on hydrocarbon productivity. Differences in fracture statistics can eventually be used as improved input into reservoir and production models. The early three-dimensional connectivity of fractures and enhanced permeability may also be critical to understanding fluid storage and migration in hydrocarbon reservoirs or seal integrity.

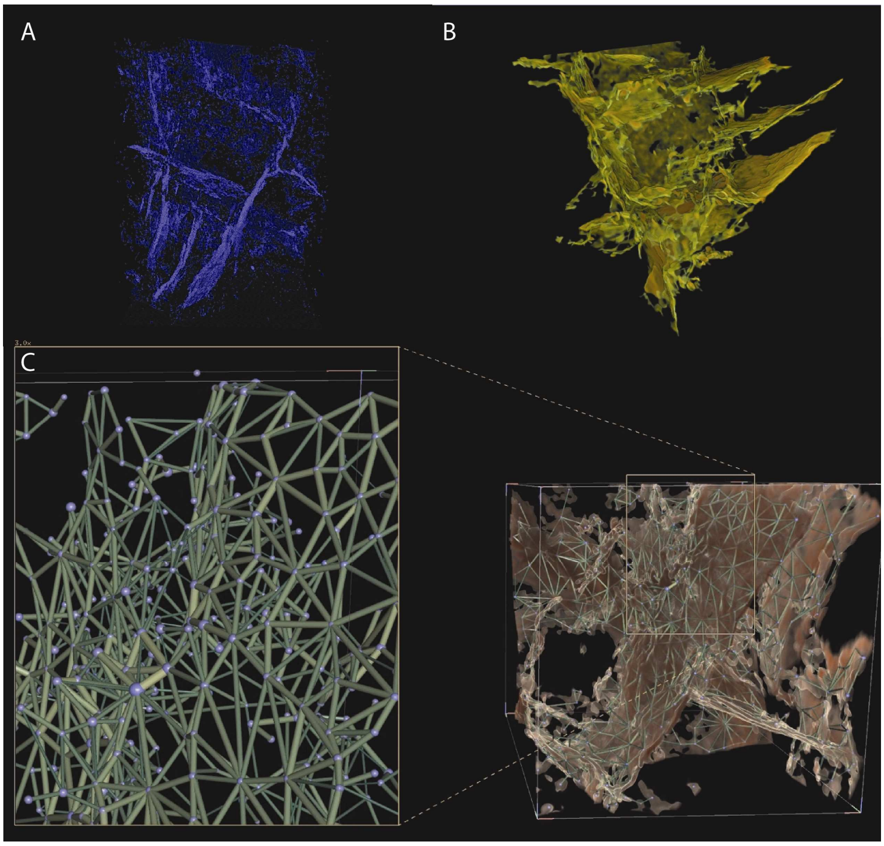

Figure 4 *3D microtomography data of a fracture network in experimentally deformed dolomite to peak stress conditions. A) raw data, B) processed and interpolated data of the voxels belonging to the fracture planes, C) Connectivity analyses shows that all the fractured area in the microtomography scan belongs to the same connected network of fractures*

References

Aydin, A. [2000]. Fractures, faults, and hydrocarbon entrapment, migration and flow. *Marine and Petroleum Geology* **17**, 797-814.

Babadagli, T. [2003]. Evaluation of EOR methods for heavy-oil recovery in naturally fractured reservoirs. *Journal of Petroleum Science and Engineering* **37**, 25-37.

Baisch, S., Weidler, R., Vörös, R., Wyborn, D., de Graf, L. [2006], Induced seismicity during the stimulation of a geothermal HFR reservoir in the Cooper Basin, Australia. *Seismological Society of America Bulletin* **96**, 2242–2256.

Barnhoorn, A., Cox, S.F., Robinson, D.J., Senden, T. [2010], Stress- and fluid-driven failure during fracture array growth: Implications for coupled deformation and fluid flow in the crust. *Geology* **38**, 779–782.

Cox, S.F. [2005], Coupling between deformation, fluid pressures, and fluid flow in ore-producing hydrothermal systems at depth in the crust, *in* Hedenquist, J.W., et al., eds., Economic Geology 100th anniversary volume: Denver, Colorado, Society of Economic Geologists, 39–75.

Curtis, J.B. [2002]. Fractured shale-gas systems. *AAPG Bulletin* **86**, 1921-1938.

Miller, S.A., Collettini, C., Chiaraluce, L., Cocco, M., Barchi, M., and Kaus, J.P. [2004], Aftershocks driven by a high-pressure CO2 source at depth. *Nature* **427**, 724–727.

Sakellariou, A., Sawkins, T.J., Senden, T.J., and Limaye, A. [2004], X-ray tomography for mesoscale physics applications. *Physica A*, **339**, 152–158.

Sibson, R.H. [2007], An episode of fault-valve behaviour during compressional inversion? The 2004 MJ 6.8 Mid-Niigata Prefecture, Japan, earthquake sequence. *Earth and Planetary Science Letters* **257**, 188–199, doi: 10.1016/j.epsl.2007.02.031.